

Spin- $\frac{3}{2}$ Pentaquark Resonance Signature in Lattice QCD

B. G. Lasscock,¹ D. B. Leinweber,¹ W. Melnitchouk,² A. W. Thomas,^{1,2}

A. G. Williams,^{1,2} R. D. Young,^{1,2} and J. M. Zanotti^{1,3}

¹ *Special Research Centre for the Subatomic Structure of Matter,
and Department of Physics, University of Adelaide, Adelaide SA 5005, Australia*

² *Jefferson Lab, 12000 Jefferson Ave., Newport News, VA 23606 USA*

³ *John von Neumann-Institut für Computing NIC/DESY, 15738 Zeuthen, Germany*

Abstract

The possible discovery of the Θ^+ pentaquark has motivated a number of studies of its nature using lattice QCD. While all the analyses thus far have focused on spin- $\frac{1}{2}$ states, here we report the results of the first exploratory study in quenched lattice QCD of pentaquarks with spin $\frac{3}{2}$. For the spin- $\frac{3}{2}$ interpolating field we use a product of the standard N and K^* operators. We do not find any evidence for the standard lattice resonance signature of attraction (i.e., binding at quark masses near the physical regime) in the $J^P = \frac{3}{2}^-$ channel. Some evidence of binding is inferred in the isoscalar $\frac{3}{2}^+$ channel at several quark masses, in accord with the standard lattice resonance signature. This suggests that this is a good candidate for the further study of pentaquarks on the lattice.

PACS numbers: 11.15.Ha, 12.38.Gc, 12.38.Aw

I. INTRODUCTION

The recent reported observations of the strangeness +1 pentaquark, Θ^+ , having minimal quark content $uudd\bar{s}$, have led to a tremendous effort aimed at understanding its properties both experimentally and theoretically. Many model studies and phenomenological analyses have explored various aspects of its structure and production mechanisms, and have at the same time have revealed a number of challenges for its interpretation as an exotic resonance with a particularly narrow width (for recent experimental reviews see Refs. [1, 2, 3, 4]).

To tackle this problem from first principles in QCD, a number of lattice studies have recently been undertaken [5, 6, 7, 8, 9, 10, 11, 12, 13, 14, 15, 16]. These have used various local spin- $\frac{1}{2}$ interpolating fields (either NK -type or diquark-diquark- \bar{s} type), and, in the case of Ref. [15], also non-local fields. Several of these studies have interpreted their results as indicating the presence of a resonance, while others report signals which are consistent with NK scattering states.

A major challenge in the lattice studies has been the identification of a resonance state from the NK scattering states. Several groups have sought to distinguish the resonance and scattering states by comparing the masses at different volumes [8, 11, 12, 14, 15]. The volume dependence of the residue of the lowest lying state has also been proposed as a way to identify the nature of the state [8, 14]. Alternatively, hybrid boundary conditions have been used in Refs. [9, 10] to differentiate the resonance in the negative parity channel from the S -wave NK scattering state.

In Ref. [5] we employed a complimentary approach to investigate spin- $\frac{1}{2}$ pentaquark resonances by searching for evidence of sufficient attraction between the constituents of the pentaquark state such that the resonance mass becomes lower than the sum of the free decay channel masses. We labeled this pattern as “the standard lattice resonance signature” because this signature is observed for conventional baryon resonances studied on the lattice [17, 18, 19, 20, 21]. By comparing the masses of the spin- $\frac{1}{2}$ five-quark states to the mass of the decay channel we found no binding at any quark mass and hence no evidence for such attraction. The absence of binding cannot be used to exclude the possibility of a resonance, as the attractive forces simply may not be strong enough to provide binding. On the other hand, the presence of binding would provide a compelling resonance signature warranting further study.

One of the major puzzles in pentaquark phenomenology has been the anomalously small width ($\lesssim 1$ MeV) observed in the experiments which have produced a positive signal. A possible explanation for this may be that if the pentaquark has $J^P = \frac{3}{2}^-$, its decay to $N + K$ must be via a D -wave, which would consequently be suppressed. In this paper we therefore extend the analysis of Ref. [5] to spin- $\frac{3}{2}$ pentaquarks. We examine both the positive and negative parity states, in both the isoscalar and isovector channels. In Sec. II we describe the interpolating field and outline the lattice techniques employed in this analysis. The results are presented in Sec. III, where we discuss in detail the mass splittings between the pentaquark and two-particle scattering states. Finally, conclusions and suggestions for future work are summarised in Sec. IV.

II. LATTICE DETAILS

A. Interpolating fields

The simplest NK -type interpolating field used in lattice simulations, referred to in Ref. [5] as the “colour-singlet” NK field, has the form:

$$\chi_{NK} = \frac{1}{\sqrt{2}} \epsilon^{abc} (u^{Ta} C \gamma_5 d^b) \{u^c (\bar{s}^e i \gamma_5 d^e) \mp (u \leftrightarrow d)\} , \quad (1)$$

where the $-$ and $+$ corresponds to the isospin $I = 0$ and 1 channels, respectively. This field has spin $\frac{1}{2}$, and transforms negatively under the parity transformation $q \rightarrow \gamma_0 q$.

One can access spin- $\frac{3}{2}$ states by replacing the spin-0 K -meson part of χ_{NK} with a spin-1 K^* vector meson operator,

$$\chi_{NK^*}^\mu = \frac{1}{\sqrt{2}} \epsilon^{abc} (u^{Ta} C \gamma_5 d^b) \{u^c (\bar{s}^e i \gamma^\mu d^e) \mp (u \leftrightarrow d)\} , \quad (2)$$

where again the $-$ and $+$ corresponds to the isospin $I = 0$ and 1 channels, respectively. The field $\chi_{NK^*}^\mu$ transforms as a vector under the parity transformation, and has overlap with both spin- $\frac{1}{2}$ and spin- $\frac{3}{2}$ pentaquark states. States of definite spin can be projected from $\chi_{NK^*}^\mu$ by applying appropriate projectors, as discussed in the next section.

B. Lattice Techniques

The masses of the spin- $\frac{1}{2}$ and spin- $\frac{3}{2}$ pentaquark states are obtained from the two-point correlation function

$$\mathcal{G}_{\mu\nu}(t, \vec{p}) = \sum_{\vec{x}} \exp(-i\vec{p} \cdot \vec{x}) \langle 0 | T \chi_{\mu}(x) \bar{\chi}_{\nu}(0) | 0 \rangle . \quad (3)$$

To project states of definite spin from the correlation function $\mathcal{G}_{\mu\nu}(t, \vec{p})$ we apply the spin projection operators [19]

$$\begin{aligned} P_{\mu\nu}^{\frac{3}{2}}(p) &= g_{\mu\nu} - \frac{1}{3}\gamma_{\mu}\gamma_{\nu} - \frac{1}{3p^2}(\gamma \cdot p \gamma_{\mu} p_{\nu} + p_{\mu} \gamma_{\nu} \gamma \cdot p) , \\ P_{\mu\nu}^{\frac{1}{2}}(p) &= g_{\mu\nu} - P_{\mu\nu}^{\frac{3}{2}}(p) , \end{aligned} \quad (4)$$

for spin- $\frac{3}{2}$ and $\frac{1}{2}$, respectively.

The spin-projected correlation function receives contributions from both positive and negative parity states. The use of fixed boundary conditions in the time direction enables states of definite parity to be projected using the matrix [18, 22]

$$\Gamma^{\mp} = \frac{1}{2} \left(1 \pm \frac{M_{B^{\pm}}}{E_{B^{\pm}}} \gamma_4 \right) , \quad (5)$$

for negative and positive parities, respectively. We note that this differs from that of Ref. [19], where interpolating fields transforming as pseudovectors, in accord with the Rarita-Schwinger spinor-vectors, were used. Masses of states with definite spin and parity can then be obtained from the spinor trace of the spin and parity projected correlation functions,

$$\begin{aligned} G(t, \vec{p}) &= \text{tr}_{\text{sp}} [\Gamma \mathcal{G}_{\mu\nu}(t, \vec{p}) P^{\nu\mu}(p)] \\ &= \sum_B \lambda^B \bar{\lambda}^B \exp(-E_B t) \\ &\stackrel{t \rightarrow \infty}{\equiv} \lambda^0 \bar{\lambda}^0 \exp(-m_0 t) . \end{aligned} \quad (6)$$

This function is a sum over all states, B , with energy E_B , and $\bar{\lambda}^B$ and λ^B are the couplings of the state B to the interpolating fields at the source and sink, respectively. Note that as in Ref. [19], we consider the case $\mu = 3$ to reduce the computational cost of the calculation.

Since the contributions to the two-point function are exponentially suppressed at a rate proportional to the energy of the state, at zero momentum the mass of the lightest state, m_0 , is obtained by fitting a constant to the effective mass,

$$M^{\text{eff}}(t) = \ln \left(\frac{G(t, \vec{0})}{G(t+1, \vec{0})} \right)$$

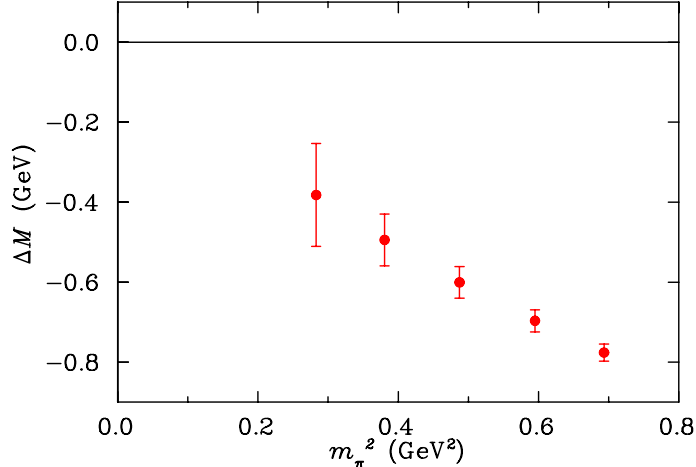


FIG. 1: Mass difference between the $I(J^P) = \frac{3}{2}(\frac{3}{2}^+)$ $\Delta(1232)$ and the P -wave $N + \pi$ decay channel.

$$\stackrel{t \rightarrow \infty}{\equiv} m_0 . \quad (7)$$

Following our previous work [5], we search for evidence that the resonance mass has become smaller than the sum of the free decay channel mass for pentaquark states created by the interpolating field $\chi_{NK^*}^\mu$. For this purpose it is useful to define an effective mass splitting. For example, in an S -wave decay channel,

$$\begin{aligned} \Delta M^{\text{eff}}(t) &\equiv M_{5q}^{\text{eff}}(t) - (M_B^{\text{eff}}(t) + M_M^{\text{eff}}(t)) \\ &\stackrel{t \rightarrow \infty}{\equiv} m_{5q} - (m_B + m_M) , \end{aligned} \quad (8)$$

where $M_B^{\text{eff}}(t)$ and $M_M^{\text{eff}}(t)$ are the appropriate baryon and meson effective masses for a specific channel. For a P -wave decay channel, the effective masses are combined with the minimum nontrivial momentum on the lattice, $2\pi/L$, to create the effective energy, $E^{\text{eff}}(t) = \sqrt{(M^{\text{eff}}(t))^2 + (2\pi/L)^2}$, for each decay particle, where L is the lattice spatial extent. The advantage of this technique is that it measures a correlated mass difference, thereby suppressing the sensitivity to systematic uncertainties (such as using different fitting ranges). Moreover, correlations in the effective masses can cancel, leading to a more accurate determination of the mass splitting.

As an example of a lattice signature of a resonance, we consider the mass splitting between the $J^P = 3/2^+$ Δ baryon and the energy of the P -wave $N + \pi$ decay channel. In Fig. 1 the typical resonance signature is clearly seen, where the Δ is bound on the lattice at heavier than physical quark masses, because of its lower energy compared with the free decay channel.

TABLE I: Lowest energy decay channels for each pentaquark state on the lattice, where the Δ baryon is bound.

$I(J^P)$	Decay channel
$0, 1(\frac{1}{2}^-)$	S -wave $N + K$
$0, 1(\frac{1}{2}^+)$	P -wave $N + K$
$0(\frac{3}{2}^-)$	S -wave $N + K^*$
$0(\frac{3}{2}^+)$	P -wave $N + K$
$1(\frac{3}{2}^-)$	S -wave $\Delta + K$
$1(\frac{3}{2}^+)$	P -wave $N + K$

For a pentaquark resonance we shall apply the same criteria, and consider the mass splittings between the pentaquark state and the corresponding baryon and meson free two-particle scattering states. The signal we are searching for is evidence of a pentaquark bound state at quark masses near the physical regime. In Table I we summarise the lowest energy decay channels for the various isospin, spin and parity quantum numbers considered in this analysis.

In the case of the Δ baryon, the binding is seen to become stronger at larger quark masses. Indeed, from their minimal quark content in the heavy quark limit, one expects to recover a Δ to $N\pi$ mass ratio of $3/5$. In the case of a pentaquark resonance, the analogous mass ratio will be 1 in the heavy quark limit and the mass splitting will vanish relative to the hadronic mass scale in the heavy quark limit. Hence a lattice resonance signature for a pentaquark state is binding (a negative mass splitting) at intermediate quark masses, above the physical regime, with a general trend of binding as a fraction of hadron mass towards zero as the heavy quark limit is approached.

C. Lattice Simulation Formalism

This analysis is based on the ensemble of 290, $20^3 \times 40$ $SU(3)$ gauge-field configurations considered in [5]. Using the mean-field $\mathcal{O}(a^2)$ -improved Luscher-Weisz plaquette plus rectangle action [23], the gauge configurations are generated via the Cabibbo-Marinari pseudoheat-bath algorithm with three diagonal $SU(2)$ subgroups looped over twice. The simulations are

performed using a parallel algorithm with appropriate link partitioning, as described in Ref. [24]. The lattice spacing is 0.128(2) fm, determined using the Sommer scale $r_0 = 0.49$ fm.

For the fermion propagators, we use the FLIC fermion action [25], an $\mathcal{O}(a)$ -improved fermion action with excellent scaling properties providing near continuum results at finite lattice spacing [26].

A fixed boundary condition in the time direction is implemented by setting $U_t(\vec{x}, N_t) = 0 \forall \vec{x}$ in the hopping terms of the fermion action. Periodic boundary conditions are imposed in the spatial directions. To explore the effects of the fixed boundary condition we have examined the effective mass of the pion correlation function and the associated χ^2_{dof} obtained in various fits. The pion is selected as it has the longest correlation length and will be a worst case scenario for the boundary effects. We find that the fixed boundary effects are completely negligible prior to time slice 30, which is the limit of signal in the pentaquark correlation functions presented below.

Gauge-invariant Gaussian smearing [27] in the spatial dimensions is applied at the fermion source at $t = 8$ to increase the overlap of the interpolating operators with the ground states. Six quark masses are used in the calculations, with $\kappa = \{0.12780, 0.12830, 0.12885, 0.12940, 0.12990, 0.13025\}$ providing $am_\pi = \{0.540, 0.500, 0.453, 0.400, 0.345, 0.300\}$ [28]. The strange quark mass is taken to be the third largest ($\kappa = 0.12885$) quark mass. This κ provides a pseudoscalar mass of 697 MeV which compares well with the experimental value of $\sqrt{2M_K^2 - M_\pi^2} = 693$ MeV motivated by leading order chiral perturbation theory. The error analysis is performed by a second-order, single-elimination jackknife, with the χ^2 per degree of freedom obtained via covariance matrix fits. Further details of the fermion action and simulation parameters are provided in Refs. [25, 26] and [5] respectively.

III. RESULTS

In this section we present our results for the masses of spin- $\frac{3}{2}$ pentaquarks for both negative and positive parity, in both the isoscalar and isovector channels.

A. Negative parity isoscalar channel

We begin the discussion of our results with the isoscalar, negative parity channel. The effect of the spin projection on the correlation function is highlighted in Fig. 2. This figure shows the effective mass plot of the $G_{33} = \text{tr}_{\text{sp}}\{\Gamma^-\mathcal{G}_{33}\}$ component of the correlation function, which contains a superposition of spin- $\frac{1}{2}$ and spin- $\frac{3}{2}$ contributions. Upon spin projection, as described by Eq. (5), two distinct states are identified.

The effective masses of the spin- $\frac{1}{2}$ and spin- $\frac{3}{2}$ states are presented in Figs. 3 and 4, respectively. To extract the masses of the lowest energy states from these effective masses, we fit over the time slices 20–30 for the spin- $\frac{1}{2}$ and 18–21 for the spin- $\frac{3}{2}$ states, respectively, where these intervals have been selected so as to obtain acceptable values of the covariance-matrix based χ^2 per degree of freedom (χ_{dof}^2), which we restrict to $\chi_{\text{dof}}^2 < 1.5$. The resulting masses are presented in Fig. 5, together with the mass of the $I(J^P) = 0(\frac{1}{2}^-)$ state extracted with the standard NK pentaquark operator [5] of Eq. (1), and the relevant (non-interacting) two-particle states. We obtain the expected result that the masses of the $I(J^P) = 0(\frac{1}{2}^-)$ state extracted with the NK and NK^* interpolators are in excellent agreement. The mass of the $I(J^P) = 0(\frac{3}{2}^-)$ state is also similar to that of the $N + K^*$ two-particle state, but lies consistently above the latter, suggesting the presence of some repulsion in this channel. Therefore we cannot conclude any evidence of a bound state in this channel.

B. Positive parity isoscalar channel

Next we consider the isoscalar state in the positive parity channel. Contrary to the negative parity signal, the spin projection shown in Fig. 6 has a less pronounced effect on the effective masses. The effective masses of the spin- $\frac{1}{2}$ and $\frac{3}{2}$ states are presented in Figs. 7 and 8, respectively. The quality of the signal in the positive parity sector is significantly reduced relative to the negative parity channel, as in the spin- $\frac{1}{2}$ analysis in Ref. [5].

The effective mass of the spin- $\frac{1}{2}$ state is fit at time slices 18–20 and the spin- $\frac{3}{2}$ state at time slices 19–24. The poor quality of the signal limits the analysis to the four largest quark masses considered. In Fig. 9 we show the fitted masses of the two spin states extracted with the NK^* interpolator. For comparison, we display the mass of the spin- $\frac{1}{2}$ state extracted with the NK interpolator, and the energies of the relevant two-particle states. Once again,

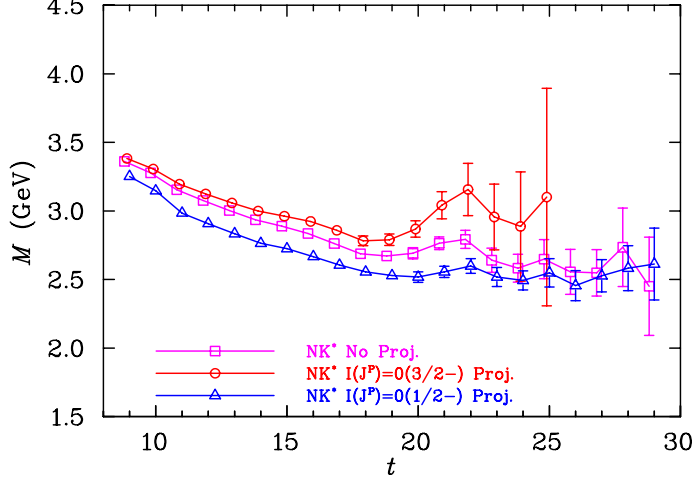


FIG. 2: Effective masses of the negative parity projected, isoscalar correlation functions calculated with the NK^* pentaquark interpolator, $\chi_{NK^*}^\mu$. The mass corresponding to the unprojected G_{33} correlation function (squares) is compared with that of the spin- $\frac{1}{2}$ (triangles) and spin- $\frac{3}{2}$ (circles) projected correlation functions. The data corresponds to our heaviest quark mass.

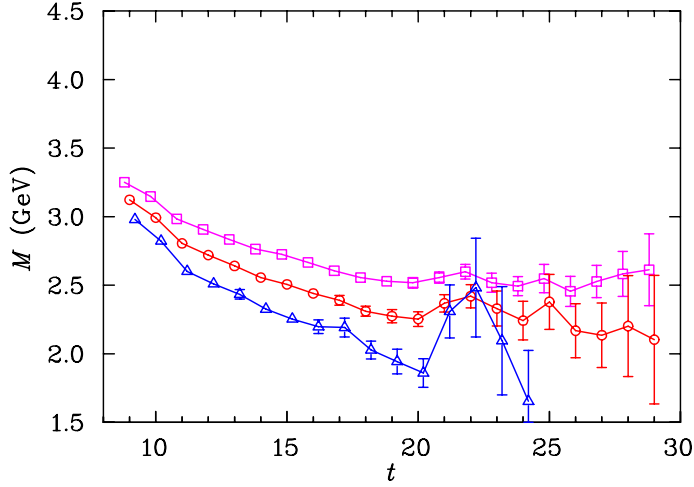


FIG. 3: Effective mass of the $I(J^P) = 0(\frac{1}{2}^-)$ pentaquark calculated with the NK^* pentaquark interpolator. The data correspond to $m_\pi \simeq 830$ MeV (squares), 700 MeV (circles), and 530 MeV (triangles).

we see excellent agreement between the masses of the spin- $\frac{1}{2}$ states extracted with the NK and NK^* interpolators.

Interestingly, the mass of the spin- $\frac{3}{2}$ state becomes *smaller* than the non-interacting two-particle energy of the P -wave $N + K$ state for intermediate quark masses, i.e., we observe

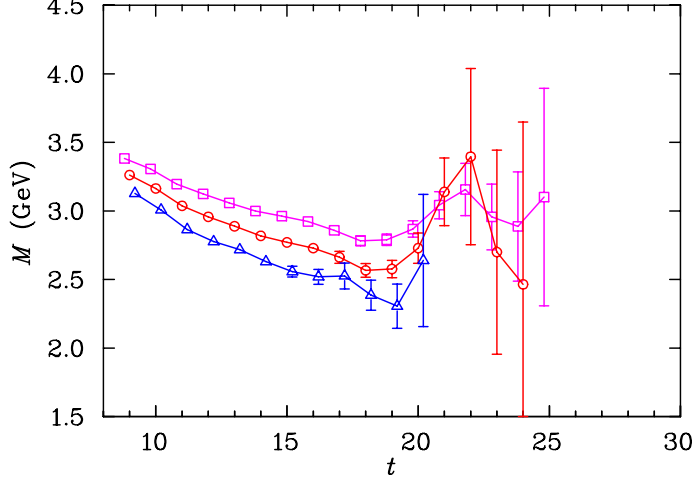


FIG. 4: As in Fig. 3, but for the $I(J^P) = 0(\frac{3}{2}^-)$ state.

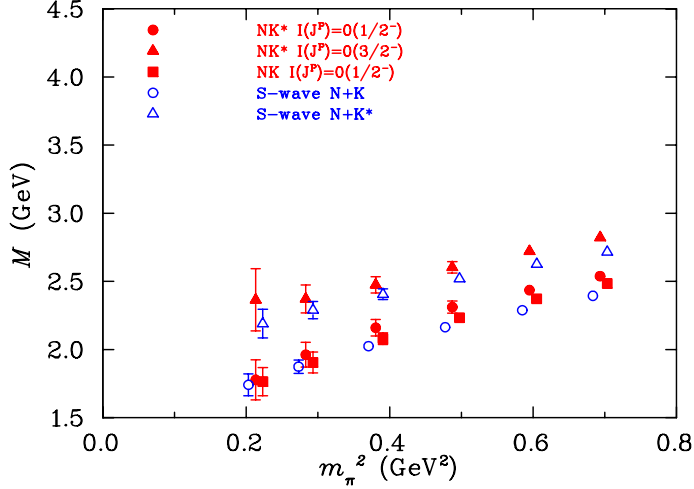


FIG. 5: Masses of the $I(J^P) = 0(\frac{1}{2}^-)$ and $0(\frac{3}{2}^-)$ states extracted with the NK^* interpolating field as a function of m_π^2 . For comparison, we also show the mass of the $I(J^P) = 0(\frac{1}{2}^-)$ state extracted from the NK pentaquark interpolator [5], and the masses of the S -wave $N + K$ and $N + K^*$ two-particle states. Some of the points have been horizontally offset for clarity.

binding. As discussed in the previous section and in Ref. [5], the transition of a resonance to a state which lies below the free particle decay channel at quark masses near the physical quark masses is the standard resonance signature in lattice QCD.

Moreover the approach to the heavy quark limit is in accord with expectations. Recall that in the case of the Θ^+ , which has a “fall-apart” decay mechanism, quark counting indicates the Θ^+ to $N + K$ mass ratio will approach 1 as the heavy quark limit is approached.

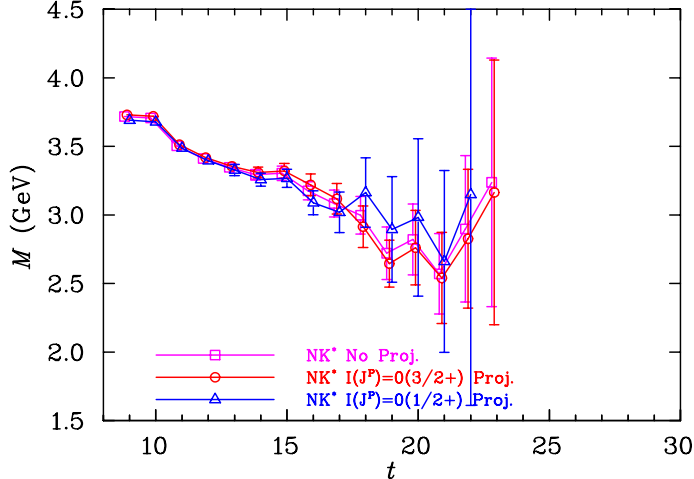


FIG. 6: As in Fig. 2, but for the isoscalar positive parity channel.

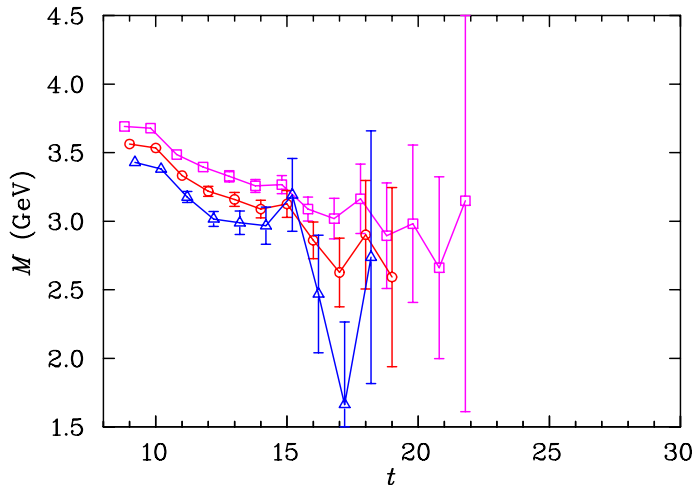


FIG. 7: Effective mass of the $I(J^P) = 0(\frac{1}{2}^+)$ pentaquark obtained from the NK^* interpolating field. The data correspond to $m_\pi \simeq 830$ MeV (squares), 700 MeV (circles), and 530 MeV (triangles).

At intermediate quark masses, however, one expects the resonance signature analogous to the Δ baryon in Fig. 1, and at the two smallest quark masses shown the pentaquark lies below the scattering state, which is the necessary condition for the presence of binding. As this result presents the possible existence of a pentaquark resonance in the physical quark mass regime, it is essential to consider a mass splitting analysis of the effective masses.

As an indicative example, we review the analysis of the lightest quark mass presented in Fig. 9. In Fig. 10 we present the effective mass splitting between the five-quark state and the lightest non-interacting two-particle state having the same quantum numbers.

At first sight it might be tempting to consider fits early in the Euclidean time evolution

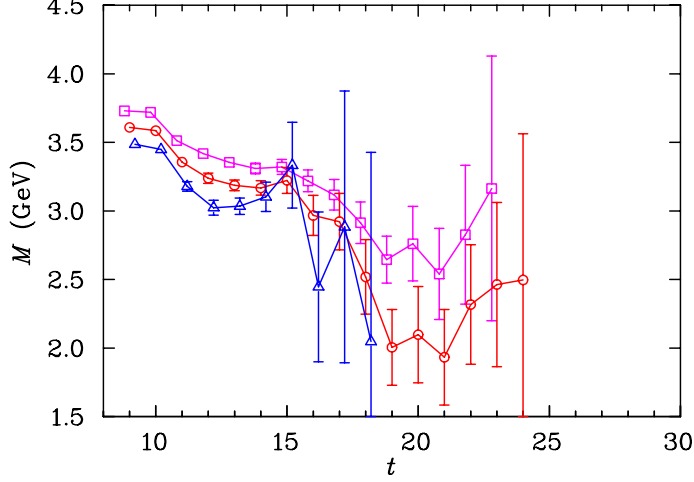


FIG. 8: As in Fig. 7, but for the $I(J^P) = 0(\frac{3}{2}^+)$ state.

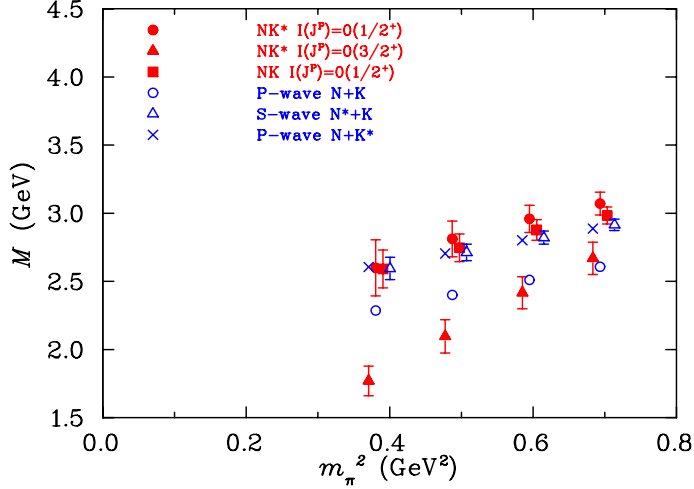


FIG. 9: Masses of the $I(J^P) = 0(\frac{1}{2}^+)$ and $0(\frac{3}{2}^+)$ states determined from the NK^* interpolating field as a function of m_π^2 . For comparison, we also show the mass of the $I(J^P) = 0(\frac{1}{2}^+)$ state extracted with the NK pentaquark interpolator [5], and the masses of the P -wave $N + K$ and $N + K^*$ and S -wave $N^* + K$ two-particle states. Some of the points have been offset horizontally for clarity.

where the errors are small and a possible plateau catches the eye. However, it is easy to demonstrate that such a fit does not describe the lowest lying state in this correlation function. For example, Fig. 11 reports the χ_{dof}^2 for a selection of fits to the effective mass shown in Fig. 10, where the lower bound of the fit window is fixed at $t = 12$ (four time steps from the source at $t = 8$), and the upper bound of the fit window is plotted on the

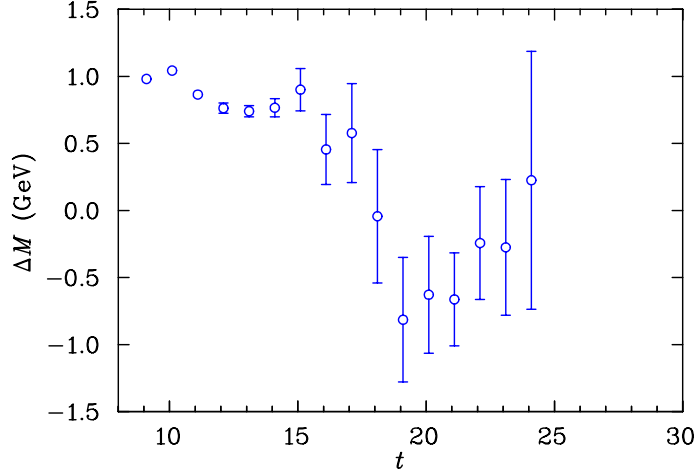


FIG. 10: Effective mass splitting between the $I(J^P) = 0(\frac{3}{2}^+)$ state extracted with the NK^* interpolator and the energy of the P -wave $N + K$ two-particle state for the lightest quark mass shown in Fig. 9.

horizontal axis. As soon as time slice 19 is included in the fit the χ_{dof}^2 becomes very large and continues to increase with the inclusion of time slices 20 and 21. One must therefore conclude that the results for time slices 19 through 21 are signal rather than noise, reflecting the true ground state of the correlator. The effective mass splitting with a “double plateau” as in Fig. 10 can occur when the interpolating fields couple strongly to a more massive state and relatively weakly to the ground state. The former dominates at early Euclidean times and the latter at later times.

To determine an appropriate lower bound for the fit, we begin by returning to Fig. 10. The fluctuation at $t = 25$ suggests that there is valid data up to time slice 24, after which noise begins to hide the signal. Indeed, the χ_{dof}^2 is approximately invariant for fits of $t = 19$ through 24 and beyond. Therefore, time slice 24 is selected for the upper bound of the fit window.

The lower bound of the fit interval must be selected with regard to the systematic time dependence of the effective mass and the χ_{dof}^2 of the fit. Figure 12 reports the latter criteria, illustrating the χ_{dof}^2 for a selection of fits to the effective mass shown in Fig. 10, where the lower bound of the fit window is shown on the horizontal axis and the upper bound of the fit window is fixed at time slice 24. The mass splittings extracted for these fits are shown in Fig. 13. Again, the lower bound of the fit window is shown on the horizontal axis and the upper bound of the fit window is fixed at time slice 24. The most statistically precise

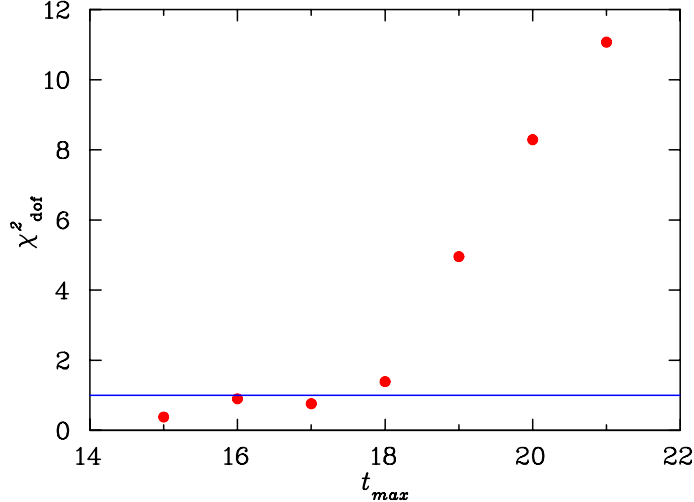


FIG. 11: The χ^2_{dof} for a series of possible fits with a lower bound fixed at time slice 12 and an upper bound shown on the horizontal axis.

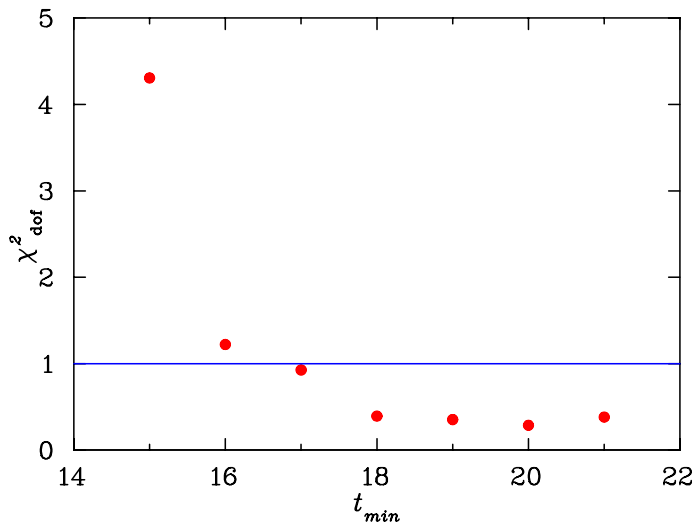


FIG. 12: The χ^2_{dof} for a series of possible fits with an upper bound fixed at time slice 24 and a lower bound shown on the horizontal axis.

estimate of the mass splitting is obtained for $t_{min} = 19$, and this result agrees with all other determinations at the 1σ level, with the exception of $t_{min} = 16$.

Having determined that there is genuine signal in the effective mass splitting at time slice 19, and given the systematic drift in the results approaching time slice 19 as illustrated in both Figs. 10 and 13, one has to conclude that nontrivial contributions from more massive excited states are still present at time slice 16. The more conservative evaluation is to delay the fit to later Euclidean times where the $\chi^2_{dof} \lesssim 1$.

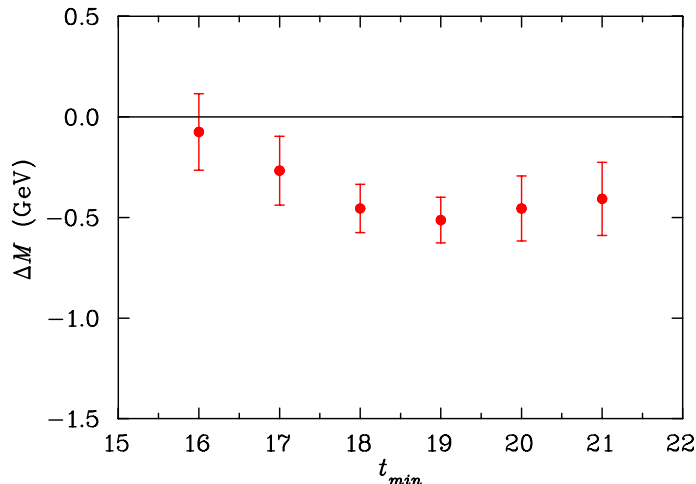


FIG. 13: Mass splitting extracted from a series of possible fits with an upper bound fixed at time slice 24 and a lower bound shown on the horizontal axis.

These χ^2_{dof} analyses have been repeated for all six quark masses considered with similar results. Figure 14 shows the mass splitting between the isoscalar spin- $\frac{3}{2}$ state extracted with the NK^* interpolator and the P -wave $N + K$ energy, where we fit at time slices 19 – 24 as concluded above. Here we are able to show the mass splitting at all of our six quark masses. The reason that we are able to recover a mass splitting for an additional two lighter quark masses is because, as discussed in the introductory section, correlated errors in the correlation functions are suppressed in constructing the effective mass splitting. The state extracted with the pentaquark operator indicates the possibility of binding for the four smallest quark masses shown.

In the infinite-volume limit, the lowest energy two-particle state, the P -wave $N + K$, approaches the energy of the S -wave $N + K$ state. As a genuine single-particle state is expected to have a small volume dependence on our lattice, we also show in Fig. 15 the mass splitting with the $N + K$ two-particle threshold. In this figure, the mass difference is also negative, as is necessary for the presence of a bound state, suggesting that the presence of binding may prevail on larger lattices. Finally, we emphasise the possibility that the mass splitting may decrease as the light quark mass regime is approached, allowing the transition to a resonance at physical quark masses. High statistics studies at lighter quark masses would obviously be of considerable interest.

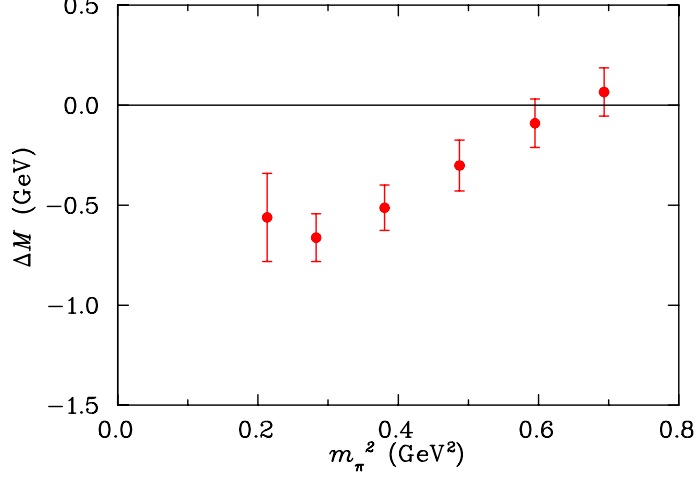


FIG. 14: Mass splitting between the $I(J^P) = 0(\frac{3}{2}^+)$ state extracted with the NK^* pentaquark interpolator and the mass of the P -wave $N + K$ energy.

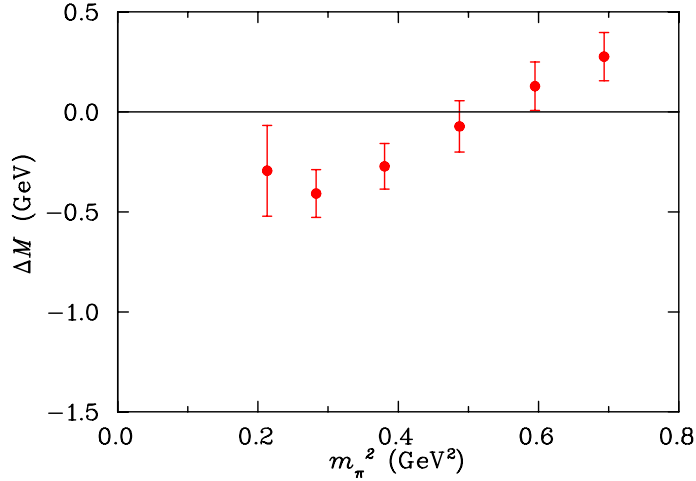


FIG. 15: Mass splitting between $I(J^P) = 0(\frac{3}{2}^+)$ state extracted with the NK^* pentaquark interpolator and the two-particle S -wave $N + K$ mass threshold.

C. Negative parity isovector channel

For completeness we also include an analysis of the isovector channel. First we present the results for the isovector, negative parity channel. In Fig. 16 we see that the effects of the spin projection for the largest quark mass are small. This may be understood by the presence of the S -wave $\Delta + K^*$ and $N + K^*$ two-particle states, which both the spin- $\frac{1}{2}$ and spin- $\frac{3}{2}$ projected correlation functions should couple to. We fit the effective masses extracted from the spin- $\frac{1}{2}$ and spin- $\frac{3}{2}$ projected correlation functions, shown in Figs. 17 and 18, at time

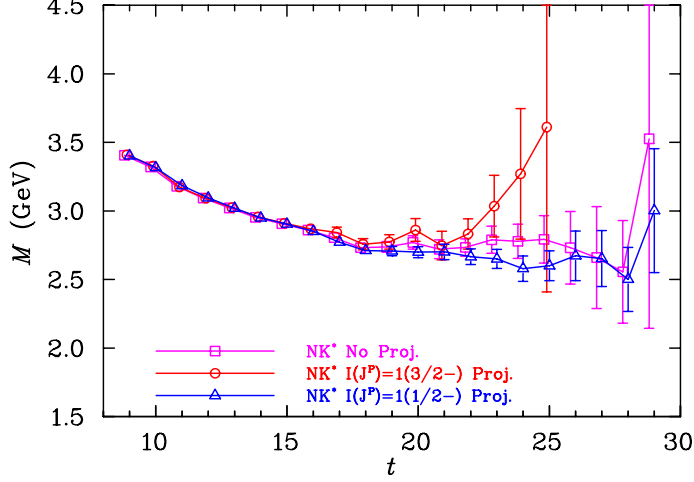


FIG. 16: As in Fig. 2, but for the isovector negative parity channel.

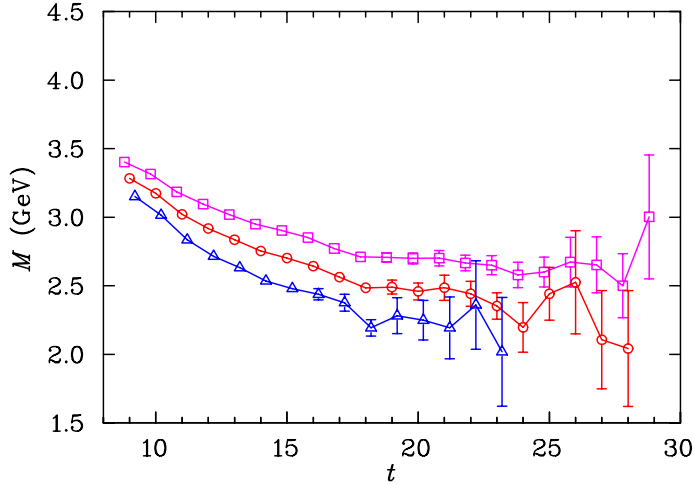


FIG. 17: Effective mass of the $I(J^P) = 1(\frac{1}{2}^-)$ pentaquark obtained for the NK^* interpolator, χ_{NK^*} . The data correspond to $m_\pi \simeq 830$ MeV (squares), 700 MeV (circles), and 530 MeV (triangles).

slices 20 – 30 and 18 – 21, respectively.

The masses are presented in Fig. 19, along with the corresponding mass extracted from the NK interpolator and the relevant two-particle states. The mass extracted from the spin- $\frac{3}{2}$ projected correlation function is in good agreement with the mass of the $N + K^*$ two-particle state. Although this correlation function must have a contribution from both the $\Delta + K$ and $N + K^*$ two-particle states, we are probably accessing an admixture of these states. A correlation matrix analysis is required to separate this admixture. The mass extracted from

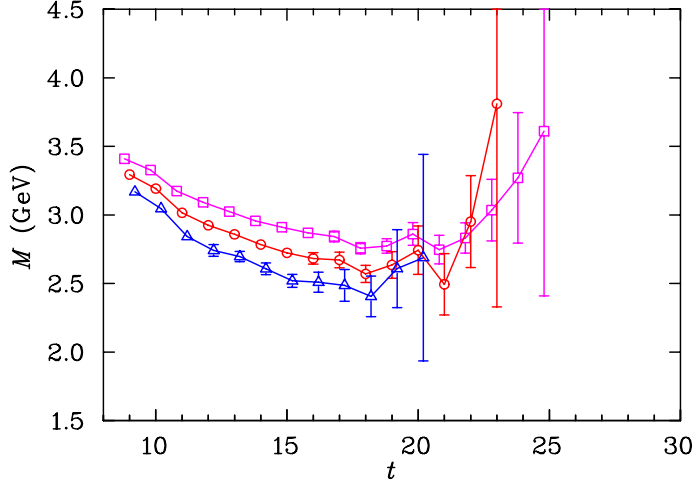


FIG. 18: As in Fig. 17, but for the $I(J^P) = 1(\frac{3}{2}^-)$ state.

the spin- $\frac{1}{2}$ projected correlation function is consistently more massive in this channel than the mass extracted with the NK interpolator. However, in Ref. [5] we used a correlation matrix to extract the mass from the NK interpolator. This process removes excited state contamination and renders the ground state mass consistently smaller. In addition, by considering the two-point functions calculated with the NK and NK^* interpolators at the quark level, one would naively expect the NK^* interpolator to couple much more strongly to the $N + K^*$ two-particle state than the NK interpolator. In fact, the weak coupling of the spin- $\frac{3}{2}$ interpolators to the lowest lying spin- $\frac{1}{2}$ states is reflected in the relatively large statistical uncertainties for the NK^* interpolator results.

In summary, as in the case of the negative parity isoscalar channel, there is no indication of the lattice resonance signature.

D. Positive parity isovector channel

Finally we complete our discussion with the positive parity isovector channel. In Fig. 20 we see that the spin projection suggests the presence of two distinct states but the errors overlap. The effective masses corresponding to these correlation functions are presented in Figs. 21 and 22. We fit the effective masses calculated from the spin- $\frac{1}{2}$ and spin- $\frac{3}{2}$ projected correlation functions at time slices 19 – 22 and 15 – 20, respectively. Due to the poor signal, results for only the three largest quark masses are shown. The masses of these states are presented in Fig. 23 along with the mass extracted with the NK interpolator and energies

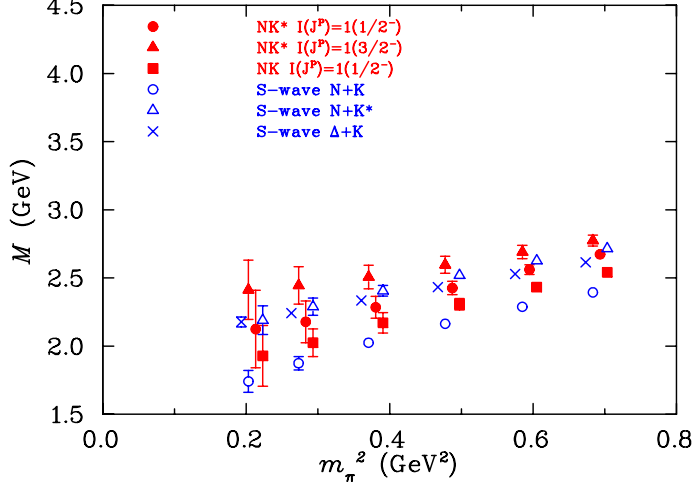


FIG. 19: Masses of the $I(J^P) = 1(\frac{1}{2}^-)$ and $1(\frac{3}{2}^-)$ states extracted with the NK^* interpolating field as a function of m_π^2 . For comparison, we also show the mass of the $I(J^P) = 1(\frac{1}{2}^-)$ state extracted with the NK pentaquark interpolator in a correlation-matrix analysis [5], and the masses of the S -wave $N + K$, $N + K^*$ and $\Delta + K$ two-particle states. Some of the points have been offset horizontally for clarity.

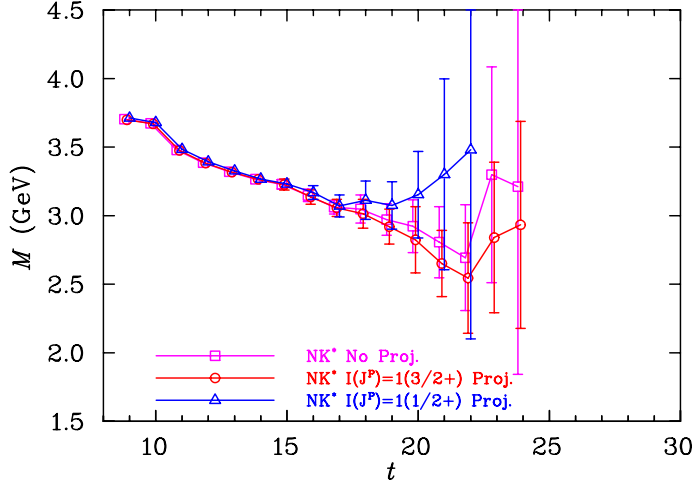


FIG. 20: As in Fig. 2, but for the isovector positive parity channel.

of the relevant two-particle states. Neither state extracted with the NK^* interpolator lies below the lowest energy scattering states, which is necessary for binding. Therefore the analogous lattice resonance signature is also absent in this channel.

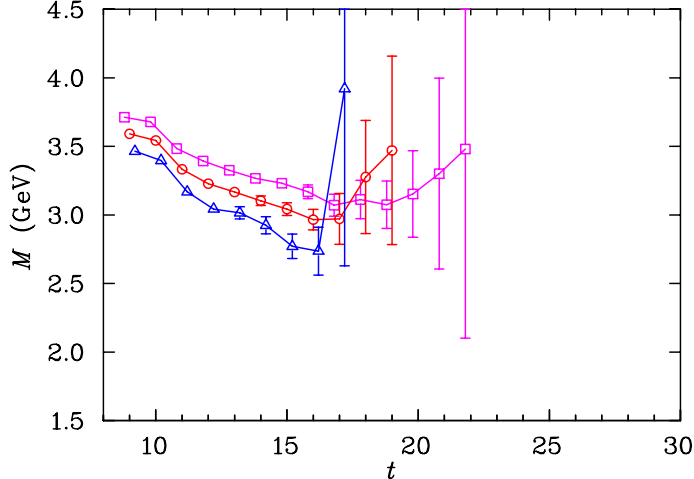


FIG. 21: Effective mass of the $I(J^P) = 1(\frac{1}{2}^+)$ pentaquark obtained from the NK^* interpolator. The data correspond to $m_\pi \simeq 830$ MeV (squares), 700 MeV (circles), and 530 MeV (triangles).

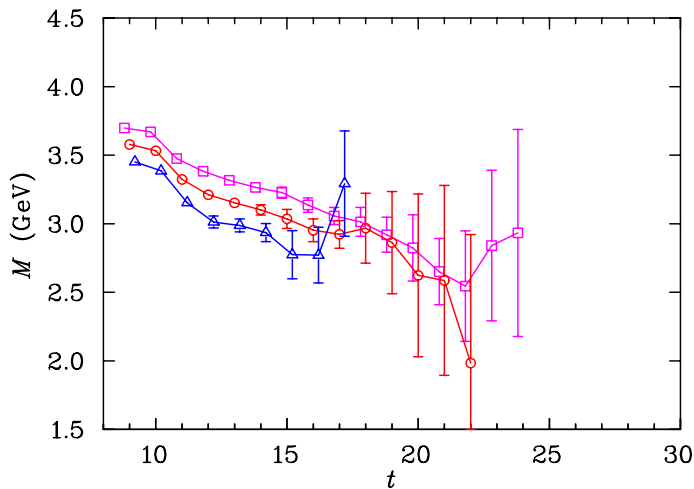


FIG. 22: As in Fig. 21, but for the $I(J^P) = 1(\frac{3}{2}^+)$ state.

IV. CONCLUSIONS

We have completed a comprehensive analysis of the isospin and parity states of the spin- $\frac{3}{2}$ pentaquark. Following our previous work [5], we search for the standard signature of a resonance in lattice QCD, where the presence of attraction renders the resonance mass lower than the sum of the free decay channel masses at quark masses near the physical regime. This standard lattice resonance signature has been observed for every conventional baryon resonance ever calculated on the lattice [17, 18, 19, 20, 21].

In the case of a pentaquark resonance, the relative mass splitting is expected to vanish in

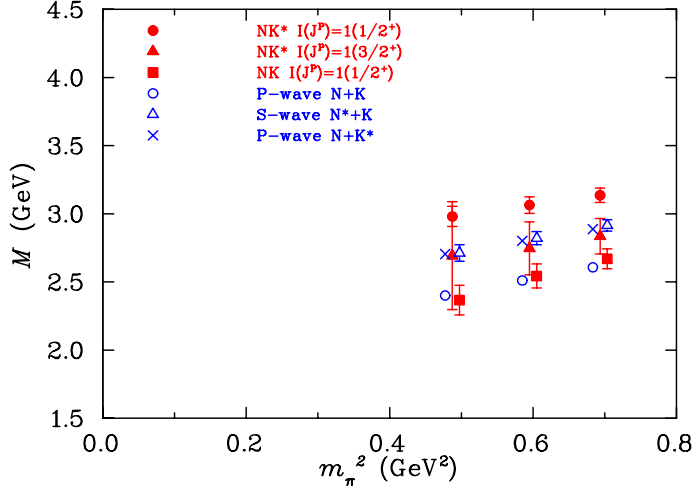


FIG. 23: Masses of the $I(J^P) = 1(\frac{1}{2}^+)$ and $1(\frac{3}{2}^+)$ states extracted with the NK^* interpolating field as a function of m_π^2 . For comparison, we also show the mass of the $I(J^P) = 1(\frac{1}{2}^+)$ state extracted with the NK pentaquark interpolator [5], and the masses of the P -wave $N + K$, $N + K^*$ and the S -wave $N^* + K$ two-particle states. Some of the points have been offset horizontally for clarity.

the heavy quark limit. Therefore the analogous lattice resonance signature for a pentaquark state will exhibit a negative mass splitting at intermediate quark masses, with a general trend towards zero as the heavy quark limit is approached.

In our examination of spin- $\frac{3}{2}$ pentaquark states we have discovered evidence of the standard lattice resonance signature, in the spin- $\frac{3}{2}$ positive-parity isoscalar channel. At intermediate quark masses, the presence of attraction between the constituents of the pentaquark baryon is sufficient to render the mass of the pentaquark state lower than the $N + K$ two-particle threshold. The mass splitting approaches zero as the light quark masses become very large, in accord with expectations. Moreover, Fig. 15 suggests that the resonance signature might prevail on larger lattices, and provides a hint that the mass splitting will decrease as the light quark mass regime is approached, allowing the transition to a resonance at physical quark masses.

Future work must explore the volume dependence of the binding observed in the spin- $\frac{3}{2}$ positive-parity isoscalar channel. Otherwise, one cannot completely rule out the possibility that the observed binding is a pure finite-volume effect, reflecting a non-trivial scattering phase shift [29] in the $I(J^P) = 0(\frac{3}{2}^+)$ NK scattering channel at momentum $p = 2\pi/L$. If

this is the case, the mass splitting will go to zero as the volume of the lattice is increased. On the other hand, a genuine single-particle state is expected to have a small volume dependence such that the negative mass splitting is preserved in the infinite volume limit. As Fig. 15 illustrates, the observed mass splitting with the $N + K$ two-particle threshold is sufficient to maintain the lattice resonance signature in the event that the volume dependence of the spin- $\frac{3}{2}$ positive-parity isoscalar state is indeed small.

The $I(J^P) = 0(\frac{3}{2}^+)$ channel is therefore an interesting pentaquark resonance candidate for further study. Chiral fermions such as the overlap fermion action [30] allowing access to the lightest quark masses [31, 32] should be brought to bear on this particular channel. High statistics studies will be vital in rendering a conclusive result. Alternative resonance signatures such as the volume dependence of the residue [8, 14] or invariance under hybrid boundary conditions [9, 10] should also be brought to bear on this most promising channel. Ultimately, it will be important to investigate the nature of this state in full QCD, where the dynamical generation of quark-antiquark pairs is accounted for in the construction of the gauge field ensemble.

Acknowledgments

We have benefited from helpful discussions with J. Dudek and K. Maltman. We thank the Australian Partnership for Advanced Computing (APAC) and the Australian National Computing Facility for Lattice Gauge Theory managed by the South Australian Partnership for Advanced Computing (SAPAC) for generous grants of supercomputer time which have enabled this project. This work was supported by the Australian Research Council, and the U.S. Department of Energy contract DE-AC05-84ER40150, under which the Southeastern Universities Research Association (SURA) operates the Thomas Jefferson National Accelerator Facility (Jefferson Lab).

-
- [1] K. Hicks (2004), hep-ex/0412048.
 - [2] K. Hicks (2005), hep-ex/0501018.
 - [3] K. H. Hicks, Prog. Part. Nucl. Phys. **55**, 647 (2005), hep-ex/0504027.
 - [4] A. R. Dzierba, C. A. Meyer, and A. P. Szczepaniak (2004), hep-ex/0412077.

- [5] B. G. Lasscock et al. (2005), hep-lat/0503008.
- [6] F. Csikor, Z. Fodor, S. D. Katz, and T. G. Kovacs, JHEP **11**, 070 (2003), hep-lat/0309090.
- [7] S. Sasaki, Phys. Rev. Lett. **93**, 152001 (2004), hep-lat/0310014.
- [8] N. Mathur et al., Phys. Rev. **D70**, 074508 (2004), hep-ph/0406196.
- [9] N. Ishii et al., Phys. Rev. **D71**, 034001 (2005), hep-lat/0408030.
- [10] N. Ishii et al. (2004), hep-lat/0410022.
- [11] T. T. Takahashi, T. Umeda, T. Onogi, and T. Kunihiro (2004), hep-lat/0410025.
- [12] T. T. Takahashi, T. Umeda, T. Onogi, and T. Kunihiro (2005), hep-lat/0503019.
- [13] T.-W. Chiu and T.-H. Hsieh (2004), hep-ph/0403020.
- [14] C. Alexandrou and A. Tsapalis (2005), hep-lat/0503013.
- [15] F. Csikor, Z. Fodor, S. D. Katz, T. G. Kovacs, and B. C. Toth (2005), hep-lat/0503012.
- [16] K. Holland and K. J. Juge (2005), hep-lat/0504007.
- [17] D. B. Leinweber, W. Melnitchouk, D. G. Richards, A. G. Williams, and J. M. Zanotti, Lect. Notes Phys. **663**, 71 (2005).
- [18] W. Melnitchouk et al., Phys. Rev. **D67**, 114506 (2003), hep-lat/0202022.
- [19] J. M. Zanotti et al. (CSSM Lattice Collaboration), Phys. Rev. **D68**, 054506 (2003), hep-lat/0304001.
- [20] S. Sasaki, T. Blum, and S. Ohta, Phys. Rev. **D65**, 074503 (2002), hep-lat/0102010.
- [21] M. Gockeler et al. (QCDSF), Phys. Lett. **B532**, 63 (2002), hep-lat/0106022.
- [22] F. X. Lee and D. B. Leinweber, Nucl. Phys. Proc. Suppl. **73**, 258 (1999), hep-lat/9809095.
- [23] M. Luscher and P. Weisz, Commun. Math. Phys. **97**, 59 (1985).
- [24] F. D. R. Bonnet, D. B. Leinweber, and A. G. Williams, J. Comput. Phys. **170**, 1 (2001), hep-lat/0001017.
- [25] J. M. Zanotti et al. (CSSM Lattice Collaboration), Phys. Rev. **D65**, 074507 (2002), hep-lat/0110216.
- [26] J. M. Zanotti, B. Lasscock, D. B. Leinweber, and A. G. Williams, Phys. Rev. **D71**, 034510 (2005), hep-lat/0405015.
- [27] S. Gusken, Nucl. Phys. Proc. Suppl. **17**, 361 (1990).
- [28] S. Boinapalli, W. Kamleh, D. B. Leinweber, A. G. Williams, and J. M. Zanotti (2004), hep-lat/0405026.
- [29] M. Luscher, Commun. Math. Phys. **105**, 153 (1986).

- [30] R. Narayanan and H. Neuberger, Phys. Rev. Lett. **71**, 3251 (1993), hep-lat/9308011.
- [31] W. Kamleh, D. H. Adams, D. B. Leinweber, and A. G. Williams, Phys. Rev. **D66**, 014501 (2002), hep-lat/0112041.
- [32] W. Kamleh, P. O. Bowman, D. B. Leinweber, A. G. Williams, and J. Zhang (2004), hep-lat/0412022.